https://doi.org/10.5194/egusphere-2023-547
Preprint. Discussion started: 1 June 2023


# Studying multi-scale ocean dynamics and their contribution to water, heat and salt budgets in the South China Sea: evaluation of a high-resolution configuration of an online closed-budget hydrodynamical ocean model (SYMPHONIE version 249).

Ngoc B. Trinh[1,2], Marine Herrmann[1,2], Caroline Ulses[1,2], Patrick Marsaleix[1], Thomas Duhaut[1], To Duy Thai[3], Claude Estournel[1], R. Kipp Shearman[4]

1. LEGOS (IRD/CNES/CNRS/UPS), 31400 Toulouse, France
2. LOTUS Laboratory, University of Science and Technology of Hanoi (USTH), Vietnam Academy of Science and Technology (VAST), Hanoi, Vietnam
3. Institute of Oceanography (IO), Vietnam Academy of Science and Technology (VAST), Nha Trang, Vietnam
4. College of Earth, Ocean, and Atmospheric Sciences, Oregon State University, Corvallis, OR, United States

Correspondence to: Ngoc Bich Trinh (trinh-bich.ngoc@usth.edu.vn)

**Short summary**

Seawater flows from the Pacific to the Indian Oceans through different straits of the South China Sea, forming the South China Sea Throughflow. We present the high-resolution model built for the study of water, heat and salt fluxes involved in this flow. The model is evaluated by comparing with observations. We moreover show that important discards are observed while calculating offline the net heat and salt flux and the inflow and outflow of water, heat and salt.

**Abstract**

The South China Sea Throughflow (SCSTF) connects the South China Sea (SCS) with neighboring seas and oceans, transferring surface water of the global thermohaline circulation between the Pacific and Indian oceans. A high resolution (4 km, 50 vertical levels) configuration of the SYMPHONIE ocean model is implemented over this region, and a simulation is performed over a 10 year period (2009 - 2018). An online computation of each term of the water, heat and salt budgets over the SCS (surface, lateral, and river fluxes and internal variations) is moreover developed. Comparisons with in-situ and satellite data show that the model reproduces correctly the spatial and temporal (from seasonal to interannual) variability of the surface water characteristics and circulation over the SCS, and the vertical distribution of water masses. The added value of an online computation compared to an offline one of water, heat and salt budget is quantitatively demonstrated. Important discards are obtained when computing heat and salt lateral fluxes offline (relative bias of respectively 31% and 52% and NRMSE of 32% and 8%, for the net heat and salt annual fluxes through the SCS). Considerable differences are also obtained for lateral incoming and outgoing fluxes, with relative

https://doi.org/10.5194/egusphere-2023-547
Preprint. Discussion started: 1 June 2023


biases of 41%, 38% and 41% and NRMSE of 352%, 226% and 338% for annual lateral inflows and outflows of water, heat and salt, respectively.

## 1. Introduction

The South China Sea (SCS, Fig. 1a), the largest marginal sea in the world, is subjected to a wide range of forcings at different scales of both natural and anthropic origins. Its coasts are among the most densely populated regions in the world (CIESIN, 2018). The SCS is a source of subsistence for these populations (fishing, tourism, etc.) and is reciprocally affected by the harmful effects of human activities (pollution, resources overexploitation, etc.). The SCS plays an important role in regional and global ocean circulation and climate, transferring the surface water masses of the global thermohaline circulation between the Pacific and Indian Oceans (Qu et al., 2005; Tozuka et al., 2007). It is therefore essential to understand, quantify and monitor the respective contributions of the lateral, atmospheric and continental fluxes in the SCS water, heat and salt budgets and their interactions.

Ocean dynamics drive the transport and mixing of water masses, and are thus strongly involved in the functioning and variability of the water, heat and salt budgets of the SCS. They also determine the fate and functioning of matter in the marine compartment (planktonic ecosystems, contaminants, sediments). The SCS ocean circulation is regulated by a combination of factors, including the geometry of the zone, the tides, the connection with the Western Pacific and Eastern Indian Oceans and the atmospheric forcing, from the daily to the seasonal and interannual scales (Wyrtki, 1961; Shaw and Chao, 1994; Metzger and Hurlburt, 1996; Gan et al., 2006). In the upper layer, the SCS basin scale circulation is mainly driven by the seasonal monsoon winds (Liu et al., 2002; Liu and Gan, 2017). In winter, strong northeasterly monsoon winds generate a cyclonic circulation in the surface and upper layers over the whole basin. In summer, weaker southwesterly monsoon winds lead to a cyclonic gyre in the north and an anticyclonic gyre in the south (Qu, 2000; Gan et al., 2016). At the interannual time-scale, the SCS circulation is impacted by the El Niño Southern Oscillation (ENSO), via its effect on monsoon winds (Soden et al., 1999; Liu et al., 2014; Tan et al., 2016) but also via the direct propagation of ENSO oceanic signals from the Western Pacific Ocean through the Luzon strait (Qu et al., 2004; Wang et al., 2006a). Other studies also suggested an impact of the Pacific Decadal Oscillation (PDO) on the SCS related to its effect on the intrusion of Western Pacific water (Yu and Qu, 2013) and on the atmospheric water flux (Zeng et al., 2018). On the other side of the spectrum, the SCS is frequently crossed by tropical cyclones (Wang et al., 2007) that affect ocean dynamics (Pan and Sun, 2013) and ecosystems (Liu et al., 2019). Last but not least, mesoscale to submesoscale structures play a significant role in the water masses dynamics and transports within the SCS (Liu et al., 2008; Nan et al., 2015; Da et al., 2019; Lin et al., 2020; Ni et al., 2021; To Duy et al., 2022).

The SCS is connected with surrounding oceans and seas by several straits (Fig. 1a, white lines). The sills of Luzon and Mindoro straits are 3000 m and 400 m deep respectively, the other straits are less than 100 m deep. The Luzon strait – the largest and deepest interocean strait of the zone – is the main pathway of seawater from the Pacific Ocean into the SCS (Wyrtki, 1961). Besides, the SCS exchanges seawater with the East China Sea through the Taiwan strait, with the Sulu Sea through the straits of Balabac and Mindoro, with the Java Sea and Andaman Sea (Indian Ocean) through Karimata and Malacca straits. Based on numerical studies, satellite observations and long-term wind data

https://doi.org/10.5194/egusphere-2023-547
Preprint. Discussion started: 1 June 2023


analyses, Qu et al. (2005) and Yu et al. (2007) revealed a circulation where Pacific Ocean water masses enter the SCS through the Luzon strait and leave the basin through the Taiwan, Karimata and Mindoro straits, forming the South China Sea Throughflow (SCSTF). Those lateral transports are involved in the SCS cycle of water, heat and salt and interact with the atmospheric and continental components of this regional cycle. The SCS indeed receives net gains of freshwater and heat from the atmosphere and rivers. Estimates of net surface heat gain vary from 17 to 51 W m$^{-2}$ (Yang et al., 1999; Qu et al., 2004; Yu and Weller, 2007; Fang et al., 2009; Wang et al., 2019) and estimates of net water gain vary between 0.05 and 0.2 Sv (Qu et al., 2006; Fang et al., 2009).

Previous estimates of water, heat and salt transports at the straits were performed based on in-situ and satellite observations (Fang et al., 1991; Chu and Li, 2000; Chung et al., 2001; Wang et al., 2003; Tian et al., 2006; Yuan et al., 2008; Fang et al., 2010; Qu and Song, 2009; Sprintall et al., 2012; Susanto et al., 2013). However, in-situ estimates remain limited in space and time and are made complicated by the complex topography in the region. Numerical modeling is a relevant tool to complement in-situ and satellite measurements. Several modeling studies based on an integrated approach considering all terms of the budgets were performed, mainly focusing on water fluxes. Yaremchuk et al. (2009) provided estimates of upper volume transport at Luzon, Taiwan, Mindoro and Karimata straits issued from a reduced - gravity model. Wang et al. (2009), using a ~18 km resolution model, evaluated the seawater fluxes through all SCS interocean straits. In both studies, the inflow at Luzon was considered to be balanced by the outflows at other straits, i.e., internal variations were neglected, and the contribution from the atmosphere and rivers was not considered. Liu et al. (2011), Hsin et al. (2012), Tozuka et al. (2015), Wei et al. (2016) provided estimates of the SCS interocean volume transports with higher resolution numerical models, but models configurations and assumptions did not allow to rigorously close the water budget. Several studies addressed the question of heat and salt fluxes. Qu et al. (2004) studied the whole depth volume transports through Luzon, Mindoro and Sunda straits and the upper heat budget of the zone, revealing that the surface heat flux is the primary heating process. However, their numerical study was carried out with a closed Taiwan strait and a shallower Mindoro strait than reality, the inflow at Luzon was balanced by outflows at Mindoro and Sunda straits, and the river heat flux was neglected. Qu et al. (2006), using a ~11 km resolution model, estimated the total volume, heat and freshwater SCSTF, deducing surface heat and freshwater transports from the difference between the inflowing and outflowing fluxes of temperature and salinity. Fang et al. (2005, 2009) were the first, followed by Wang et al. (2019), to evaluate transports through all interocean straits of the SCS, using respectively ~18 km then ~7 km resolution models, but assuming that outflows compensate for inflows.

Those studies considerably improved our understanding of water, heat and salt transport through the SCS area. However, they were associated with several limitations. First, they assumed that the SCS is at equilibrium over the studied periods, i.e., that the same amount of water, heat and salt that enters the basin leaves it, and used this assumption to deduce atmosphere and rivers contributions. Though this assumption allows to close the budget at the first order, it does not account for possible internal variations and trends in the water, heat and salt contents of the SCS. Yet Zeng et al. (2014, 2018), using in situ measurements and satellite data, evidenced a freshening of the SCS from 2010 to 2012 followed by a salinification until 2016, suggesting an interannual variability in salt and/or water

https://doi.org/10.5194/egusphere-2023-547
Preprint. Discussion started: 1 June 2023


mass content. Moreover, very few studies examined jointly the water, heat and salt budgets, which is however necessary to provide consistent estimates of all the terms involved in those budgets and understand their interactions. Last, the model resolution was rarely finer than 10 km, not allowing to fully represent the (sub)mesoscale structures involved in the SCS circulation (Da et al. 2019, Herrmann et al. 2023).

Following this introduction, our first scientific objective is to better understand the role of the SCS in the global circulation and regional climate at different scales, i.e., daily, seasonal and interannual variability, by providing updated and consistent estimates at those scales of all the terms involved in the SCS volume, heat and salt budgets: lateral, atmospheric and river fluxes and internal variations. For that, we developed a configuration of a regional ocean hydrodynamical model with a high spatial resolution (4 km) over the SCS, to represent as realistically as possible the wide range of scales of the processes involved in the SCS dynamics. The water, heat and salt budgets have been rigorously closed by performing online calculations of each term of those budgets, including incoming and outgoing flows. The objective of this paper is to present and evaluate in detail this modeling tool, that will be used first to study water, salt and heat budgets, and will be available to the community interested in addressing scientific questions related to SCS ocean dynamics functioning, variability and influence.

The paper is organized as follows. Sect. 2 presents the hydrodynamical model, its high-resolution configuration over the SCS and the observation data used for its evaluation. The online computation of each term of the budgets are then detailed. The ability of the model to simulate the SCS dynamics and water masses at different scales is evaluated in Sect. 3. The added-value of the online computation of volume, heat, and salt budgets compared to the offline computation is analyzed in Sect. 4. Results are summarized in Sect. 5, and an overview on the future applications of this high-resolution closed-budget modeling tool is provided.

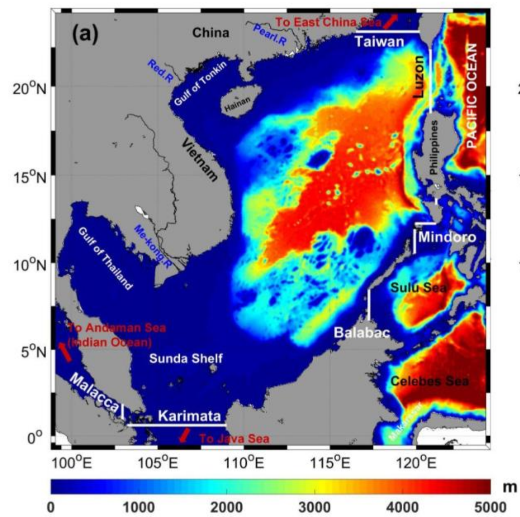


**Figure 1.** (a) Computational domain bathymetry and interocean straits (white lines). (b) Maps of Argo float trajectories in the SCS from January 2009 to December 2018 (red), TSG from R/V Alis trajectory from May to July 2014 (blue), and Glider trajectory from January to May 2017 (green).

## 2. Materials and methods

### 2.1 The numerical model SYMPHONIE

#### 2.1.1 General presentation of the model

The 3-D ocean circulation model SYMPHONIE Marsaleix et al. (2008, 2019) is based on the Navier-Stokes primitive equations solved on an Arakawa curvilinear C-grid under the hydrostatic and Boussinesq approximations. The model makes use of an energy conserving finite difference method (Marsaleix et al., 2008), a forward-backward time stepping scheme, a Jacobian pressure gradient scheme (Marsaleix et al., 2009), the equation of state of Jackett et al. (2006), and the K-epsilon turbulence scheme with the implementation described in Costa et al. (2017). Horizontal advection and diffusion of tracers are computed using the QUICKEST scheme (Leonard, 1979) and vertical advection using a centered scheme. Horizontal advection and diffusion of momentum are each computed with a fourth order centered biharmonic scheme. The biharmonic viscosity of momentum is calculated according to a Smagorinsky-like formulation derived from Griffies and Hallberg (2000). The lateral open boundary conditions, based on radiation conditions combined with nudging conditions, are described in Marsaleix et al., (2006) and boundary conditions at river mouths are described in Nguyen-Duy et al. (2021). As in Estournel et al. (2021), To Duy et al. (2022) and Hermann et al. (2023), the VQS (vanishing quasi-sigma) vertical coordinate is used, allowing to avoid an excess of

https://doi.org/10.5194/egusphere-2023-547
Preprint. Discussion started: 1 June 2023


vertical levels in very shallow areas while maintaining an accurate description of the bathymetry and to reduce the truncation errors associated with the sigma coordinate.

#### 2.1.2 Model setup

The SYMPHONIE numerical configuration covers the whole SCS (from 99°E to 124°E and from -0.6°N to 24°N, Fig. 1a), with a regular grid of 4 km horizontal resolution and 50 vertical levels in the deepest area. It is built from a bathymetry product merging GEBCO 2014 gridded bathymetry and digitalized nautical charts (Piton et al., 2020). Bathymetry ranges from 3 m to 5000 m in the studied area (Fig. 1a). The simulation runs from 01 January 2009 to 31 December 2018.

Initial and lateral boundary conditions for temperature, salinity, currents and sea level are provided by the daily outputs of the Global_Analysis_Forecast_Phy_001_024 Global Ocean 1/12° physics analysis and forecast provided by Copernicus Marine Environment Monitoring Service (CMEMS) (http://marine.copernicus.eu; last access 18 May 2023).

The SCS configuration includes 63 river mouths. Daily data were provided by the National Hydro-Meteorological Service of Vietnam for 11 rivers flowing in northern and central Vietnam (including the Red river). Monthly climatology runoff issued from the CLS – INDESO project were provided for the other rivers, including the Mekong river and Pearl river (Tranchant et al., 2016).

The atmospheric forcing is calculated from the bulk formulae of Large and Yeager (2004) using the European Centre for Medium Range Weather Forecasts (ECMWF) operational forecasts at 1/8° horizontal resolution and 3 hours temporal resolution, available at https://www.ecmwf.int/, last access 18 May 2023.

Open boundary tidal conditions are prescribed from FES2014b, the 2015 release of the FES (Finite Element Solution) global tide model (Carrere et al., 2012). The data are freely available at the Aviso website: https://www.aviso.altimetry.fr/en/data/products/auxiliary-products/global-tide-fes.html (last access 18 May 2023). The SCS configuration takes into account nine barotropic tidal components (in phase and altitude): M2, S2, N2, K2 (semi-diurnal tides), K1, P1, O1, Q1 (diurnal tides) and M4 (compound tide). The model is also forced by the astronomical plus the loading and self-attraction potentials (Lyard et al., 2006). Details and numerical issues related to tides can be found in Pairaud et al. (2008, 2010).

### 2.2 Fluxes calculation methods

We detail here the computation of each term of the volume, heat and salt budgets over the whole SCS: internal content variations and surface, lateral and river fluxes. We compute lateral fluxes through the six interocean straits connecting the SCS to neighboring seas and oceans shown in Fig. 1a: Taiwan, Luzon, Mindoro, Balabac, Karimata and Malacca straits. All the terms of the budget equations are computed online. The added-value of the online computation compared to the offline computation is presented in Sect. 4.

#### 2.2.1 Volume, heat and salt balances equations

***Water volume balance***

https://doi.org/10.5194/egusphere-2023-547
Preprint. Discussion started: 1 June 2023


The internal variation of water volume V over the SCS area between times $t_1$ and $t_2$ ($\Delta V$) is equal to the integral between $t_1$ and $t_2$ of all water fluxes into (out of) the SCS domain, taken as the sea zone limited by the six interocean straits shown in Fig. 1a:

$$\Delta V = V_{t2} - V_{t1} = \int_{t_1}^{t_2} (F_{w,lat} + F_{w,surf} + F_{w,riv})dt \qquad \text{(Eq. 1)}$$

where $F_{w,lat}$, $F_{w,surf}$ and $F_{w,riv}$ are the net lateral, surface and river water fluxes respectively. Here and in the following, positive lateral fluxes correspond to inflows, and negative fluxes to outflows

***Heat balance***

The variation of heat content *HC* between times $t_1$ and $t_2$ ($\Delta HC$) is equal to the sum of all heat fluxes exchanged within the SCS domain between $t_1$ and $t_2$:

$$\Delta HC = HC_{t2} - HC_{t1} = \int_{t_1}^{t_2} (F_{T,lat} + F_{T,surf} + F_{T,riv})dt \qquad \text{(Eq. 2)}$$

where $F_{T,lat}$, $F_{T,surf}$ and $F_{T,riv}$ are the net lateral, surface and river heat fluxes respectively, and HC is computed from:

$$HC = \rho_0 C_p \int_x \int_y \int_z T(x,y,z,t)dx\,dy\,dz \qquad \text{(Eq. 3)}$$

with *T* the temperature (in °C), $\rho_0$ the seawater density constant (1028 kg $m^{-3}$), $C_p$ the seawater specific heat constant (3900 $J kg^{-1} {}^{\circ}C^{-1}$).

***Salt balance***

We assume that there is no salt input from surface atmospheric fluxes and river runoff and that the only source/sink of salt is from the lateral boundaries. The variation of salt content between $t_1$ and $t_2$ ($\Delta SC$) is thus equal to the sum of salt fluxes exchanged at the lateral boundaries of the SCS domain:

$$\Delta SC = SC_{t2} - SC_{t1} = \int_{t_1}^{t_2} F_{S,lat}dt \qquad \text{(Eq. 4)}$$

where $F_{S,lat}$ is the net salt flux at the lateral boundaries and SC is computed from:

$$SC = \rho_0 \int_x \int_y \int_z S(x,y,z,t)\,dx\,dy\,dz \qquad \text{(Eq. 5)}$$

with S the salinity.

### 2.2.2 Lateral volume, heat and salt fluxes

The total lateral volume flux $F_{w,lat}$ through the vertical section A is computed in Sv (1 Sv = $10^6$ $m^3 s^{-1}$) from:

$$F_{w,lat} = \int_A v_t\,dA \qquad \text{(Eq. 6)}$$

with $v_t$ the current velocity normal to the transect and *A* the area of the section from the surface to bottom.

The lateral heat flux $F_{T,lat}$ in PW (PW =$10^{15}$ W) is computed from:

$$F_{T,lat} = \rho_0 C_p \int_A T v_t dA \qquad \text{(Eq. 7)}$$

The lateral salt flux $F_{S,lat}$ in Gg $s^{-1}$ is computed from:

https://doi.org/10.5194/egusphere-2023-547
Preprint. Discussion started: 1 June 2023


$$F_{S,lat} = \rho_0 \int_A S v_t dA \qquad \text{(Eq. 8)}$$

Inflowing and outflowing fluxes are also computed using the same equations, but for values of $v_t > 0$ and $v_t < 0$, respectively:

$$F_{w,lat+} = \int_A v_t \,/\, (v_t > 0)\, dA \text{ and } F_{w,lat-} = \int_A v_t \,/\, (v_t < 0)\, dA \qquad \text{(Eq. 6')}$$

$$F_{T,lat+} = \rho_0 C_p \int_A T v_t \,/ (v_t > 0)\, dA \text{ and } F_{T,lat-} \rho_0 C_p \int_A T v_t \,/ (v_t < 0)\, dA \qquad \text{(Eq. 7')}$$

$$F_{S,lat+} = \rho_0 \int_A S v_t \,/\, (v_t > 0)\, dA \text{ and } F_{S,lat-} = \rho_0 \int_A S v_t \,/\, (v_t < 0)\, dA \qquad \text{(Eq. 8')}$$

### 2.2.3 Atmospheric (surface) fluxes

The atmospheric freshwater flux is computed in Sv (1 Sv = $10^6$ $m^3$ $s^{-1}$) from:

$$F_{w,surf} = \int_{Surf} (P - E) dxdy \qquad \text{(Eq. 9)}$$

where P stands for the precipitation in m $s^{-1}$, E the evaporation in m $s^{-1}$, Surf is the SCS area limited by the six interocean straits shown in Fig. 1a.

The net surface heat flux ($F_{T,surf}$), in PW, is the sum over the SCS of the short-wave radiation flux ($F_{SR}$), long-wave radiation flux ($F_{LR}$), sensible heat flux ($F_{SEN}$) and latent heat flux ($F_{LATENT}$):

$$F_{T,surf} = \int_{Surf} (F_{SR} + F_{LR} + F_{SEN} + F_{LATENT}) dxdy \qquad \text{(Eq. 10)}$$

### 2.2.4 River fluxes

The river flux $F_{w,riv}$ is calculated as the sum over all the rivers of the product of the velocity of river flow at the river mouth, $v_{riv}$:

$$F_{w,riv} = \sum_{rivers} \int_A v_{riv} dA \qquad \text{(Eq. 11)}$$

where A is the area of the river mouth section from the surface to the bottom.
The river heat flux $F_{Triv}$, in PW, is computed from:

$$F_{T,riv} = \sum_{rivers} \rho_0 C_p \int_A T\, v_{riv}\, dA \qquad \text{(Eq. 12)}$$

where T is the temperature (in °C) at the river mouth.

Finally, it should be noted that the flux calculations are numerically consistent with those carried out by the model through the advection scheme and its surface and continental boundary conditions. Along these lines, $C_p$ and $\rho_0$ constants correspond to the values used by the bulk formulas and the horizontal fluxes are calculated in the same way as in the advection scheme of the model. This allows to produce a strictly closed balance: the sum of all fluxes explains 100% of the variations of the volume and of the total heat and salt contents at each time step of the simulation, as will be shown in Sect. 4.

### 2.3 Observational datasets

Satellite data are used for evaluating the representation of ocean surface characteristics (SST, Sea Surface Temperature; SSS, Sea Surface Salinity; SLA, Sea Level Anomaly). In-situ data are used to evaluate the surface and vertical representation of water mass properties and the mixed layer depth (MLD).

#### 2.3.1 Satellite data

To evaluate the modeled SST, we use daily OSTIA (Operational Sea Surface Temperature and Sea Ice Analysis) outputs for the period 2009 – 2018, available at https://data.nodc.noaa.gov/ghrsst/L4/GLOB/UKMO/OSTIA/ (last access 18 May 2023). OSTIA is a GHRSST (Group for High Resolution Sea Surface Temperature) Level 4 SST daily product built from multiple spatial sensors and drifting and moored buoys data, with a horizontal resolution of 1/18°. Regarding the SSS, we use outputs from the 9-day-averaged de-biased SMOS (Soil Moisture and Ocean Salinity) SSS Level 3 version 3, developed by Boutin et al. (2016). It has a resolution of 25 km and is available for the period 2010 – 2017. Data are distributed by the CECOS (Ocean Salinity Expertise Center) and the CNES - IFREMER CATDS (Centre Aval de Traitement des Données SMOS) via: https://data.catds.fr/cecos-locean/Ocean_products/L3_DEBIAS_LOCEAN/ (last access 18 May 2023). To evaluate the SLA and surface geostrophic currents, we use daily 1/4° global ocean gridded L4 sea surface heights in delayed – time of CMEMS, available at: https://data.marine.copernicus.eu/product/SEALEVEL_GLO_PHY_L4_MY_008_047/description (last access 18 May 2023). This altimetry product (hereafter called ALTI) is generated using data from different altimeter missions and covers the period from 1993 up to present (Ablain et al., 2015; Ray and Zaron, 2016). For model-data comparison, we extracted the daily altimetric SLA on the period of simulation (2009 – 2018) and removed at each point of each dataset (model and altimetry) the temporal average over 2009 - 2018.

#### 2.3.2 In-situ data

More than 12 600 Argo profiles were collected in the SCS between 2009 and 2018 (see Fig. 1b), available from https://data-argo.ifremer.fr/geo/pacific_ocean/ (http://doi.org/10.17882/42182, last access 18 May 2023)..

The ALIS R/V crossed the SCS from 10 May to 28 July 2014 (see Fig. 1b), measuring SST and SSS every 6 s by the vessel-mounted Seabird SBE21 thermosalinometer (hereafter called TSG-Alis data).

Under the framework of a cooperative Vietnam - US international research program (Rogowski et al., 2019), a Seaglider sg206 was deployed on 22 January 2017 until 16 May 2017 in the SCS (see Fig. 1b). It collected 555 vertical profiles of conductivity, temperature and pressure from an unpumped Sea-Bird Electronics CTD (SBE 41CP). Conductivity, temperature and depth were sampled at 5 s intervals in the upper 150 m, corresponding to a resolution finer than 1 m, and between 55 – 100 s below. All sensors were factory calibrated. Salinity was corrected for the thermal lag error using a variable flow rate (Garau et al., 2011).
Argo, TS-Alis and glider in-situ measurements are compared in Sect. 4 with modeled profiles at the nearest point (in position and time).

https://doi.org/10.5194/egusphere-2023-547
Preprint. Discussion started: 1 June 2023


### 2.4. Statistical evaluation

The simulated dataset S and observational dataset O (of the same size N) are compared using three statistical parameters: the bias, the Normalized Root Mean Square Error (NRMSE) and the Pearson correlation coefficient R:

$$Bias = \overline{S} - \overline{O} \qquad \text{(Eq. 13)}$$

$$NRMSE = \frac{\sqrt{\frac{1}{N}\sum_{i=1}^{n}(Si-Oi)^2}}{(O_{max}-O_{min})} \qquad \text{(Eq. 14)}$$

$$R = \frac{\sum_{i=1}^{N}(O_i-\overline{O})(S_i-\overline{S})}{\sum_{i=1}^{N}(O_i-\overline{O})^2\sum_{i=1}^{N}(S_i-\overline{S})^2} \qquad \text{(Eq. 15)}$$

Where Si and Oi are respectively the simulated and observed series, and $\overline{S}$ and $\overline{O}$ their mean values. In Sect. 4, we use the same statistical evaluation methods for the comparison between online and offline computation on lateral fluxes: $S_i$, $O_i$, $\overline{S}$ and $\overline{O}$ are respectively replaced by $OF_i$ (the offline fluxes series), $ON_i$ (the online fluxes series), $\overline{OF}$ and $\overline{ON}$ (the corresponding mean values).

## 3. Model evaluation

In this section, we evaluate the ability of the simulation performed over 2009-2018 to simulate the hydrological and hydrodynamical SCS characteristics.

### 3.1 Tides

The tide representation is evaluated by comparing numerical results with the tidal atlas FES2014b, also used to provide the tidal forcing. We show in Fig. 2 the observed and simulated tidal amplitude and phase for K1, O1, M2 and S2, the four principal tidal components in the SCS region. The SCS is indeed one of the few regions of the global ocean where diurnal tides (K1, O1) dominate semi-diurnal tides (M2, S2) (Guohong, 1986). The spatial distribution of tidal constituents obtained from the model and from FES2014b is similar to the study of Phan et al. (2019). Diurnal tides prevail over the Gulf of Tonkin, the Gulf of Thailand and the southwestern SCS. Mixed tides (mainly semi-diurnal tides) prevail along southern China, the northwest coast of Borneo and the continental shelf of the Mekong delta. For those four tidal components, we obtain a strong similarity both for amplitudes and phases between the model and FES2014b over most of the modeled domain. The most noticeable weaknesses are a small (< 10 cm) overestimation of diurnal (K1 and O1) amplitude and overestimation (~20 cm) of semi-diurnal (M2 and S2) amplitude in the Sulu Sea, and a small overestimation of K1 amplitude off the Mekong Delta. The bias of semi-diurnal tidal amplitudes in the Sulu Sea may be related to the prescribed bathymetry in the area, with many small islands separating this area from the surrounding seas.

https://doi.org/10.5194/egusphere-2023-547
Preprint. Discussion started: 1 June 2023


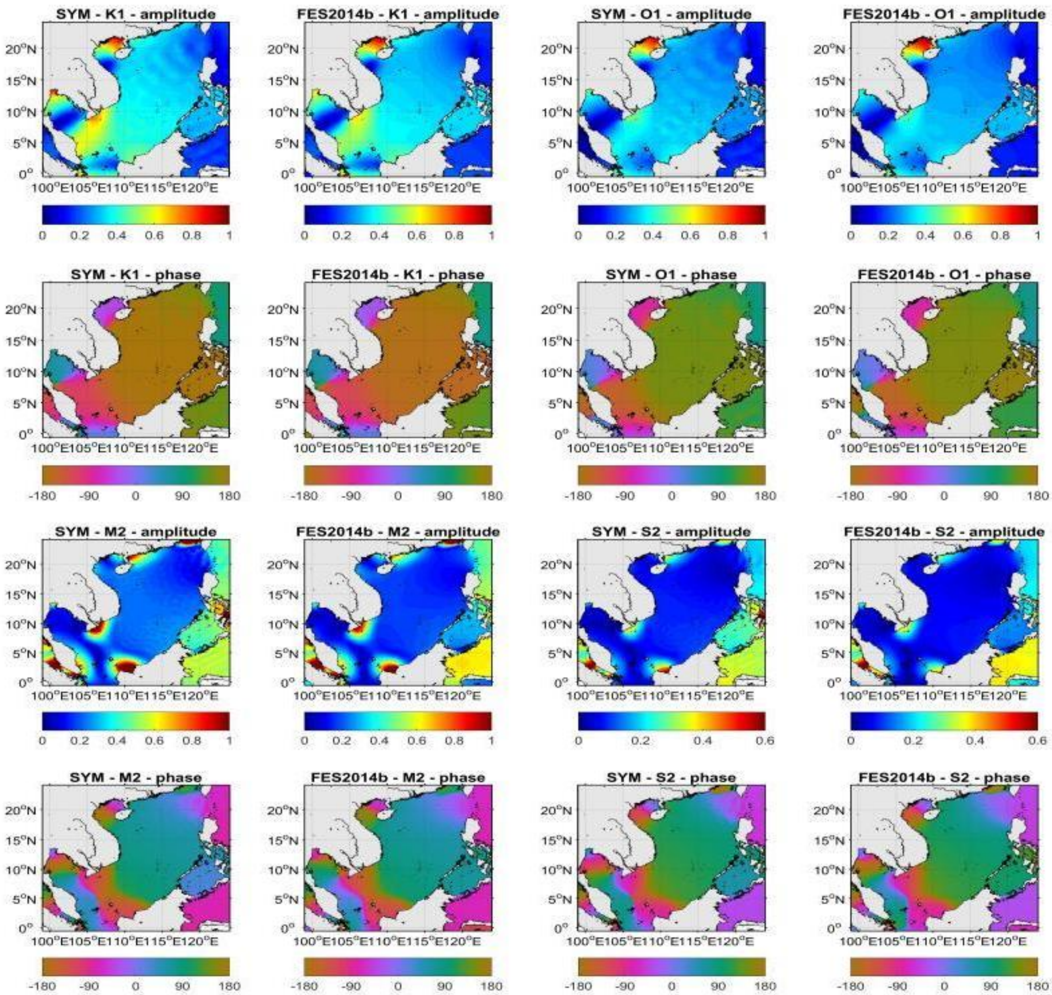


**Figure 2.** Amplitude (m) and phase (degree) of four tidal components K1, O1, M2, S2 in the model (SYM) and the global tidal product FES2014b.

### 3.2 Surface characteristics

For the evaluation of each sea surface characteristics (SST, SSS and SLA), we present below the comparison between model outputs and corresponding satellite observations over 2009-2018 for the seasonal cycle (Fig. 3a,c,e), the interannual variations (Fig. 3b,d,f) and the seasonal spatial distributions (Fig. 4).

https://doi.org/10.5194/egusphere-2023-547
Preprint. Discussion started: 1 June 2023


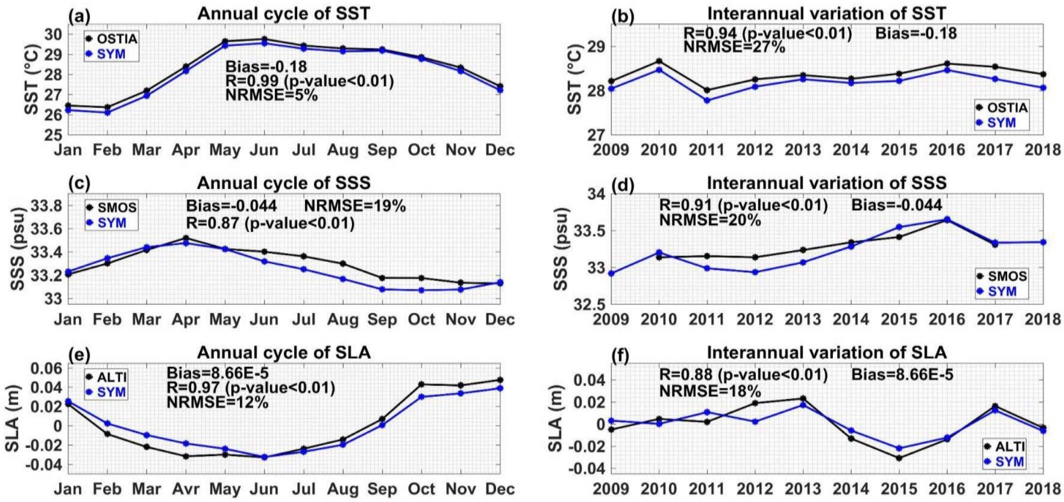


**Figure 3.** Time series of climatological monthly mean (left) and yearly mean (right) over 2009-2018 of SST (°C, a, b), SSS (psu, c, d) and SLA (m, e, f) averaged over the SCS domain, computed from the model (SYM, blue) and from satellite observations (OSTIA, SMOS and ALTI, black).

### 3.2.1 Annual cycle

The SST annual cycle (Fig. 3a) is very well simulated, with a highly significant correlation (R=0.99 and p-value $p < 0.01$, corresponding to a significant level higher than 99%), and a small NRMSE (0.05) between the model outputs and OSTIA, and a slight bias of -0.18°C. In both datasets, the monthly climatological cycle of SST reaches its maximum value in May/June (spring-summer) and decreases to its minimum in January/February (winter). This monthly climatological SST agrees with the study of Kumar et al. (2010), who observed the same SST annual cycle by analyzing hydrographic WOA data (World Ocean Atlas, 2005).

The simulated SSS seasonal cycle (Fig. 3c) also shows a good agreement with SMOS data, with a highly significant correlation of 0.89 ($p < 0.01$), a low NRMSE equal to 19%, and a slight negative bias (-0.04). In both model and data, the average SSS is maximum in April (spring) with values of 33.47 in the model and 33.52 in SMOS, and minimum from September to December (autumn) with 33.07 in the model and 33.17 in SMOS. This significant seasonal variation of SSS in the SCS, with high salinity in winter-spring and low salinity in summer-autumn was also obtained by Kumar et al. (2010) and Zeng et al. (2014).

The annual cycle of SLA obtained with the model and ALTI data during the period 2009 - 2018 shows a minimum value in spring-summer (June) with -0.033 m both for the model and ALTI (Fig. 3e). The SLA reaches its highest value in winter (December) with 0.039 m and 0.049 m respectively for the model and ALTI. The model outputs and the altimeter measurements have a highly significant correlation (R=0.97, $p<0.01$), and a small NRMSE value (0.12). The simulated monthly climatological SLA is also in agreement with Shaw et al. (1999) and Ho et al. (2000): using

https://doi.org/10.5194/egusphere-2023-547
Preprint. Discussion started: 1 June 2023


TOPEX/Poseidon altimeter data, they both concluded on a higher SLA in winter and lower SLA in summer over the SCS.

### 3.2.2 Interannual variations

We obtain a highly significant correlation coefficient between the model and OSTIA (R=0.94, p<0.01) regarding yearly SST interannual variations (Fig. 3b). The yearly SST bias (-0.18 °C in average) is nearly constant over the period and the NRMSE is 27%. From 2009 to 2018, the averaged yearly SST over the basin reaches its highest values in 2010 and 2016 (28.47°C and 28.46°C respectively). This is consistent with the study of Yu et al. (2019), who found a co-occurrence between those SST positive anomalies peaks and El-Niño events in 2009-2010 and 2015-2016 (see the NOAA ONI time series available at https://origin.cpc.ncep.noaa.gov/products/analysis_monitoring/ensostuff/ONI_v5.php). The minimum of averaged SST (27.77°C) occurs in 2011, corresponding to the 2011-2012 La Niña event. Yu et al. (2019) obtained the same interannual time-series by analyzing MODIS satellite-derived SST data for the period 2003 - 2017.

The simulated interannual variations of yearly SSS (Fig. 3d) show a highly significant correlation (R=0.91, p<0.01) and a rather low NRMSE value (20%) with satellite data. There is a significant increase of the annual averaged SSS over the SCS between 2012 to 2016, both in the model outputs and SMOS data. Over the period 2010 - 2017, the SSS reaches a low value in 2012 (32.93 for the model, 33.14 for SMOS), then increases continuously until a maximum value in 2016 (33.65 for the model, 33.64 for SMOS). The freshening until 2012 and strong salinification during the following four years are in agreement with observations of Zeng et al. (2014, 2018), who revealed that 2012 was the year with the lowest recorded value of SSS in the SCS over a 50-year period, and that the SSS then increased from late 2012 to 2016.

In terms of SLA interannual variations, our model and ALTI show strong similarities with a NRMSE equal to 18% (Fig. 3f) and a highly significant correlation (R=0.88, p<0.01). During the studied period, the overall averaged SLA is maximum in 2013 (0.017 m in model outputs and 0.023 m in ALTI), and minimum in 2015 (-0.02 m in the model and -0.03 m in ALTI).

### 3.2.3 Spatial seasonal surface patterns

In this section we compare the simulated and observed maps of SST, SSS and SLA averaged over the boreal winter (December, January and February, DJF) and summer (June, July and August, JJA) over 2009-2018 (Fig. 4).

https://doi.org/10.5194/egusphere-2023-547
Preprint. Discussion started: 1 June 2023


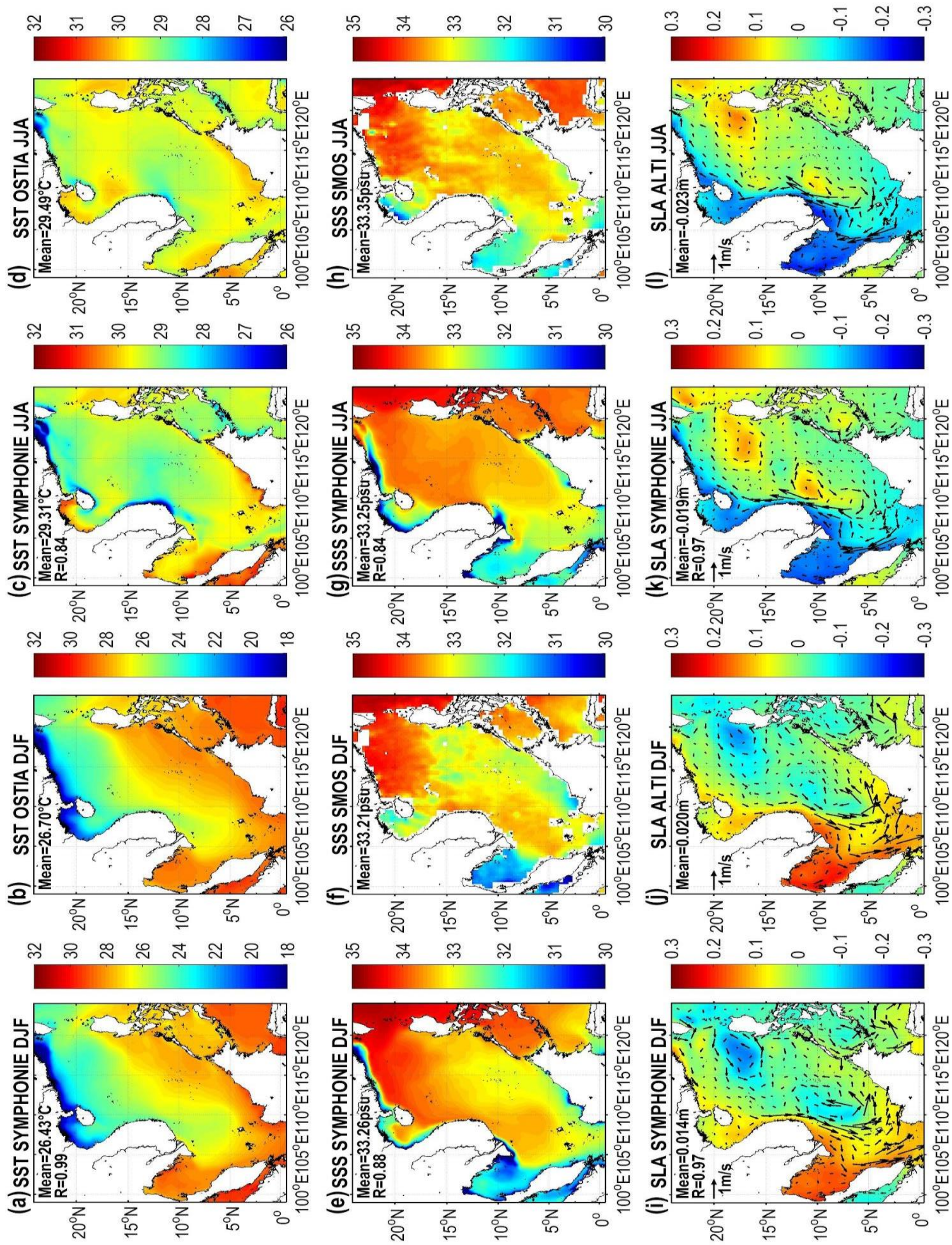


349

350 **Figure 4.** Spatial distribution of winter (DJF) and summer (JJA) climatologically averaged SST (°C, a, b, c, d), SSS (psu, e, f, g, h), SLA (m) and geostrophic current (m/s, i, j, k, l) in model outputs and corresponding satellite observations. R stands for the spatial correlation coefficient (here p-value is always smaller than 0.01).

https://doi.org/10.5194/egusphere-2023-547
Preprint. Discussion started: 1 June 2023


In both winter and summer, the simulated SST is very close to observations, with highly significant spatial correlation (respectively R=0.99 and 0.84 in winter and summer, p<0.01) and similar ranges compared to OSTIA (Fig. 4 a,b). In winter, the model shows an average negative bias of -0.27 °C, and colder zones offshore southern Vietnam and in the northern basin. In summer (Fig. 4 c,d), the average negative bias is reduced to -0.18 °C, and the simulation produces a SST colder than OSTIA in the northern SCS near Taiwan, off southern Vietnam coast, along the Mekong delta, and in the Sulu and Celebes seas (see Fig. 1a). On the other hand, simulated SST is warmer in the Gulf of Tonkin, Gulf of Thailand and the southern basin.

The simulated spatial distribution of SSS also shows a highly significant spatial correlation with SMOS for both seasons (R=0.88 and 0.84 in winter and summer, respectively, p<0.01). The model has a positive bias in winter (0.05), and a negative bias in summer (-0.1). In winter (Fig. 4 e,f), the Chinese and Vietnam coastal zones and the Gulf of Thailand are fresher in the model than in SMOS data, whereas the center of the basin and the southern Gulf of Tonkin are saltier. In summer (Fig. 4 g,h), we obtain a significantly lower SSS at the big river mouths (Pearl River, Red River, Mekong River), in the Gulf of Thailand and in the Malacca strait in model outputs compared to SMOS. SMOS, with a resolution of 25 km, might however not be able to capture these salinity changes in the coastal zone.

Both in winter and summer, the simulated and observed seasonal mean spatial distributions of SLA show a highly significant correlation (R=0.97, p<0.01, Fig. 4 i,j,k,l). The model shows very weak negative seasonal biases in SLA compared to ALTI (-0.006 m in winter and -0.004 m in summer). In the Gulf of Thailand, the simulated SLA is lower in winter and higher in summer compared to ALTI. Regarding the geostrophic currents, we obtain great similarities between the model and ALTI. In winter when the northeastern monsoon dominates, two cells of cyclonic gyre cover the whole basin, one near Luzon and another at the Sunda shelf. In summer, with the southwest monsoon, most of the SCS geostrophic currents reverse and flow northeast. The geostrophic currents are most intense at the Sunda shelf zone (see Fig. 1a) in winter. In summer, we observe strong geostrophic flows at the southern Vietnam coast, and at the east of the Malaysian coast. The intensity and direction of those seasonal geostrophic currents are consistent with previous studies (e.g., Da et al., 2019; Wang et al., 2006b).

Last, Fig. 5i,j shows the observed TSG-Alis SST and SSS during spring-summer 2014 and the corresponding colocalized simulated SSS and SST. Again, the simulation shows a strong similarity with TSG-Alis data, with correlation coefficients of 0.70 and 0.82 (p<0.01), for SST and SSS respectively, during this 6th year of the simulation.

Those comparisons between simulated and observed SST, SSS and SLA time series and spatial fields show that our simulation realistically reproduces the annual cycle and interannual variations and the seasonal spatial distributions of SCS surface hydrological characteristics and circulation over the period 2009-2018.

### 3.3 Water mass characteristics

We hereafter examine the performance of the model in simulating the vertical distribution of water masses properties. For that, we compare model results with Argo and glider observations. Fig. 5a-h show the colocalized simulated and observed temperature and salinity profiles, their mean value and the bias between model and data.

We obtain a strong agreement between the simulated and observed temperature and salinity profiles both for Argo floats (over the period 2009-2018) and glider (winter-spring 2016) outputs (Fig. 5a-h). In particular the maximum salinity observed in the intermediate water mass, corresponding to the Maximum Salinity Water (MSW), is well reproduced by the model. In general, modeled temperatures are lower than measured temperatures, with a negative bias in the whole water column (Fig. 5b,f). The highest biases are located in the subsurface layer (50-200 m), with maximum biases of -1.2°C compared to Argo data and of -1.5°C compared to glider data. Under 200 m, the temperature bias is stable, varying around 0.2-0.5°C compared to Argo floats, and 0.7-1°C compared to glider data. Model results show a general very low positive salinity bias compared to Argo and glider data below 200 m. A higher salinity bias is obtained in the subsurface layer: 0.2 psu compared to Argo data (Fig. 5d) and 0.3 psu compared to glider data (Fig. 5h). Our simulation therefore represents realistically the various SCS water masses characteristics over the water column.

Argo floats, glider and model produce water masses characteristics in agreement with previous studies done on water masses over the SCS (Uu and Brankart, 1997; Penjan et al., 1997; Rojana-anawat et al., 1998; Saadon et al., 1998a, b) and the Pacific (Talley et al., 2011) (Fig. 5a-h). In the upper layer (0-50 m), we observe both the Open Sea Water (OSW), characterized by salinities of 33-34 and temperatures of 25-30 °C, and the Continental Shelf Waters (CSW) with low salinities (< 33) and temperatures between 20 and 30°C (depending on the season). The 50-100 m layer is characterized by the mixing between the Northern Open Sea Water (NOSW) and the Pacific Ocean Water (POW) during winter. The NOSW has salinities of 34-34.5 and temperatures of 23-25 °C. The POW is saltier with salinities of 34-35 and temperatures of 25-27 °C. Deeper, at 100-200 m, the MSW is characterized by temperatures between 15-17 °C and salinities between 34.5 and 35 and is a property of the equatorial regions (Rojana-anawat et al., 1998). Below the MSW, from 200-1000 m, the North Pacific Intermediate Water (NPIW) and Pacific Equatorial Water (PEW) are flowing with temperatures and salinities between 5-13 °C and 34-35, respectively. The Deep Water (DW), below 1000 m, is identified by temperatures of 2-5 °C, and salinities of 34.3 - 34.7. Temperature profiles located in the Sulu Sea do not follow those characteristics in the deep layers, both in Argo and model outputs, showing temperature varying from 7 to 10°C below 700 m. This marginal sea, nearly isothermal, indeed possesses unique water characteristics, with a potential temperature varying around 9.8°C below 1000 m (Wyrtki, 1961; Chen et al., 2006; Gordon et al., 2011), much higher than those of neighboring seas such as the SCS, the Celebes Sea and the Western (Qu and Song, 2009).

https://doi.org/10.5194/egusphere-2023-547
Preprint. Discussion started: 1 June 2023


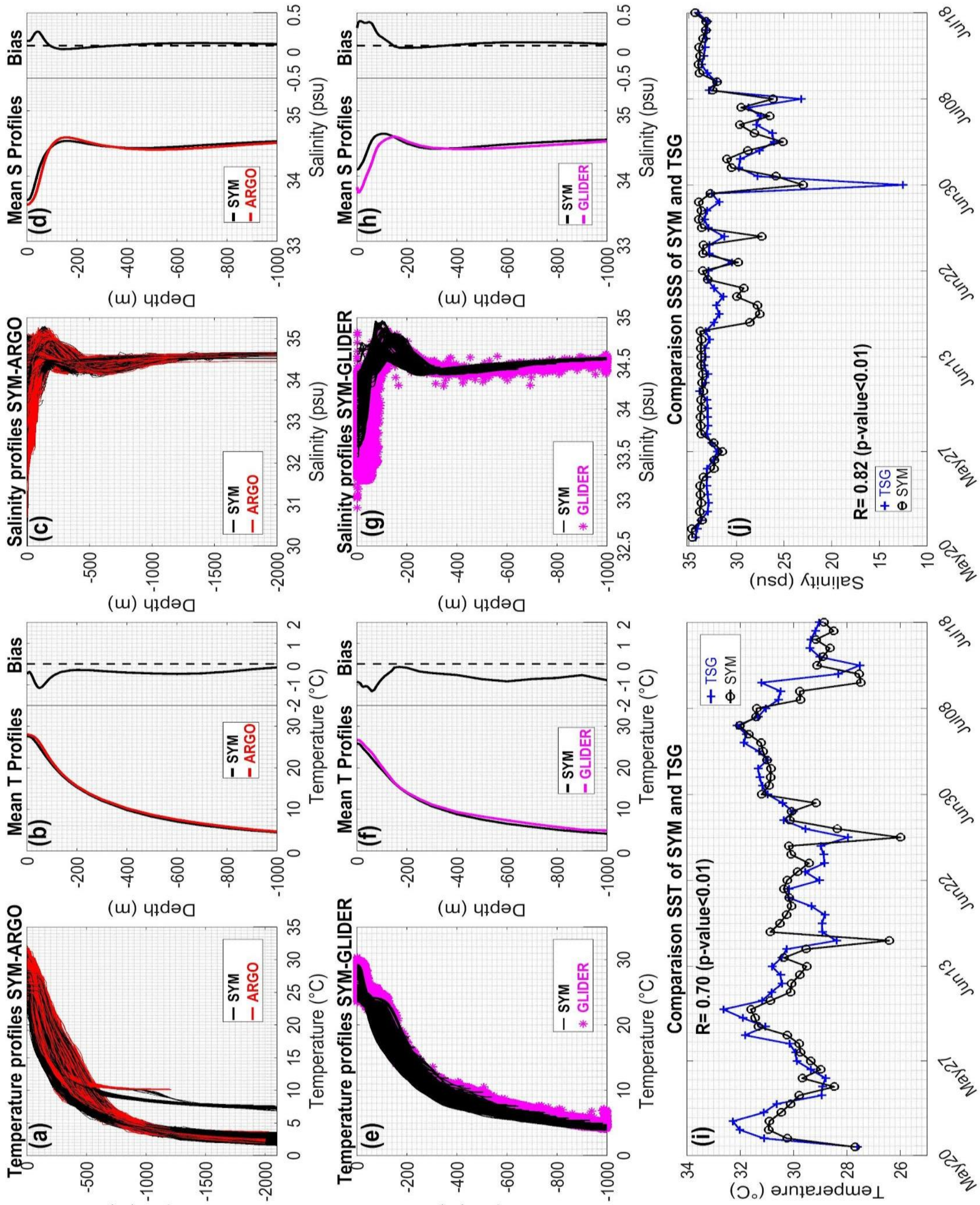


**Figure 5.** (a to h) Temperature (°C) and salinity vertical profiles (all profiles, mean profiles and mean bias between model and observations) from model outputs (black), Argo floats (a,b,c,d, red) and glider measurements (e,f,g,h, magenta). (i,j) SST (°C) and SSS from the model (black) and TSG-Alis data (blue) .

https://doi.org/10.5194/egusphere-2023-547
Preprint. Discussion started: 1 June 2023


### 3.4 Mixed layer depth

The seasonal distribution of simulated mixed layer depth (MLD) in the SCS basin is evaluated by comparison with values computed from Argo profiles. The MLD is calculated based on a 0.5 °C temperature criteria, corresponding to the temperature difference between the near-surface and the MLD. Figure 6 shows the winter (DJF) and summer (JJA) spatial distributions of the colocalized simulated and observed MLD at Argo locations (in space and time), as well as the simulated and observed time series of monthly mean MLD averaged over the Argo points over the SCS.

Spatial distributions of the simulated MLD are close to observed values. Observed and simulated MLD are deeper in winter (varying between ~80 m in the north and ~30 m in the east, Fig. 6a,b) and shallower in summer (varying between ~50 m in the south and ~20 m in the north, Fig. 6d,e). The simulated MLD in both seasons are in general shallower than MLD obtained from Argo profiles, with bias locally reaching -20 m in DJF (Fig. 6c,f). This shallower MLD explains the slightly temperature underestimation and salinity overestimation around ~50 m depth (Fig. 5b,d). The average bias over the area and period is equal to -9.5 m (Fig. 6g), and is stronger for higher values of MLD in winter (e.g. ~-40 m in January 2021). This bias is stable over the 10 years of simulation (Fig. 6g), indicating that there is no drift in terms of simulated MLD. Moreover, the observed temporal variability of MLD is well reproduced by the model, with a 0.91 ($p<0.01$) highly significant correlation between the simulated and observed monthly MLD.
The underestimation of simulated MLD, stronger for higher values of MLD, could be partly related to the underestimation of wind speed over the area. Regional atmospheric models indeed underestimate sea surface wind speed over the region, especially for periods and areas of strong winds (Herrmann et al., 2020, 2021). Figure 7 shows the average sea surface wind speed observed by QuikSCAT and simulated by ECMWF analysis (used to prescribe the atmospheric forcing to the model) over their common period (2008): it reveals an underestimation of ~-1m.s$^{-1}$ of sea surface wind speed in ECMWF.

https://doi.org/10.5194/egusphere-2023-547
Preprint. Discussion started: 1 June 2023


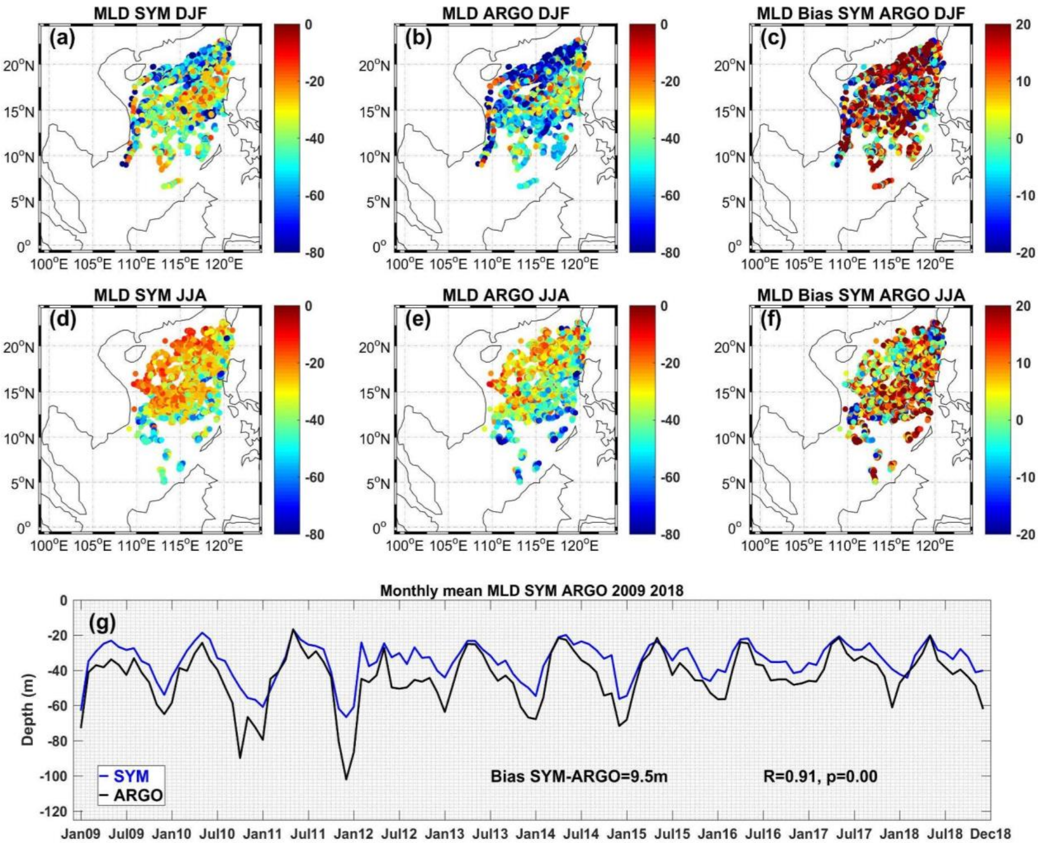


**Figure 6**: Seasonal distribution of MLD (m) from (a,c) the model and (b,d) Argo data and their bias (c,f) in winter (1st row) and summer (2nd row); (g) time series of monthly MLD (m) averaged over the domain in the model and Argo data over the period 2009 - 2018.

https://doi.org/10.5194/egusphere-2023-547
Preprint. Discussion started: 1 June 2023


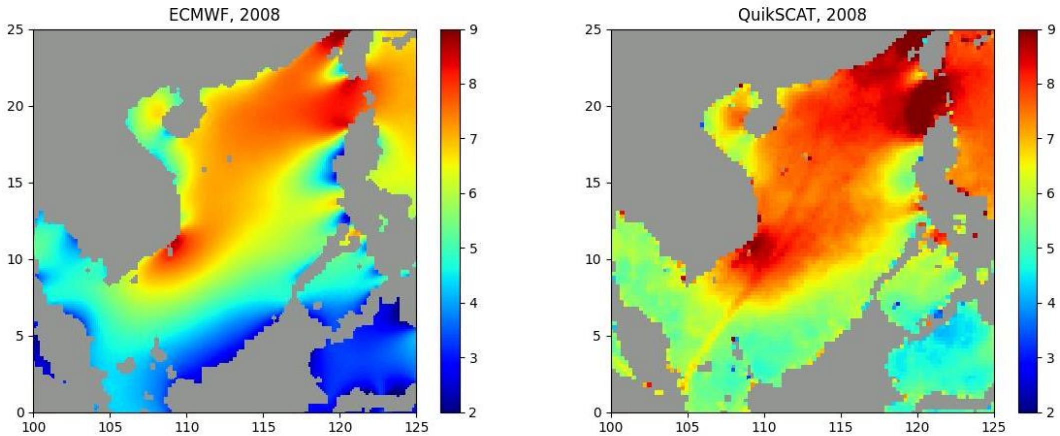


**Figure 7**: Sea surface wind speed (m $s^{-1}$) over the SCS averaged over the year 2008 computed from ECMWF 3-hourly analysis outputs (left) and daily QuikSCAT outputs (right).

## 4. Added-value of the online budget computation

Computing online all the terms of the budget allows to calculate the exact net lateral fluxes through each lateral boundary hence to rigorously close the budgets at all time scales, but also to calculate the exact outflowing/inflowing fluxes at each time step. Here we quantitatively show the added value of the online computation of water, heat and salt budgets compared to the offline computation. Computing the lateral term offline, using the modeled velocity, temperature and salinity at the output frequency, relies on the assumption that the integral over the output period of the product of velocity and temperature (or salinity) is equal to the product of their integrals, thus that the turbulent term $\overline{u'T'}$ in the following equation is negligible:

$$\overline{uT} = \overline{(\bar{u} + u')(\bar{T} + T')} = \overline{\bar{u}\bar{T}} + \overline{u'\bar{T}} + \overline{T'\bar{u}} + \overline{u'T'} = \bar{u}\bar{T} + \overline{u'T'} \qquad \text{(Eq. 16)}$$

where u is the velocity normal to the vertical section and T the temperature at this point, and the overbar stands for the integral over the output period.

In Fig. 8a,b,c we show each term of the budget equation for the annual variation of volume, heat and salt contents over the SCS, computed online and offline: annual variation, atmospheric surface fluxes, river fluxes, lateral fluxes and the sum of all fluxes, that should equal the annual variation. Table 1 provides the values of net, inflowing and outflowing annual fluxes computed online, and the bias, correlation and NRMSE between the offline and online computations. First, those figures confirm that when computed online, the sum of annual fluxes is equal to the annual variation, i.e., that the budget equation is closed in our model. This is shown here for the interannual variation but is also verified at each time step of the whole simulation (figure not shown). Second, Fig. 8a,b,c quantitatively highlight the error induced when neglecting the turbulent term in Eq. 16 by computing the lateral net fluxes offline. For the volume flux, using the online (blue) and offline (cyan) computation for net lateral fluxes is equivalent since it does not imply any non-linear assumption. For the heat and salt fluxes however, the difference is significant: we obtain

https://doi.org/10.5194/egusphere-2023-547
Preprint. Discussion started: 1 June 2023


NRMSE of, respectively, 32% and 8% between the online and offline computations for, respectively, heat and salt net lateral fluxes over the SCS for the 2009-2018 period (Table 1).

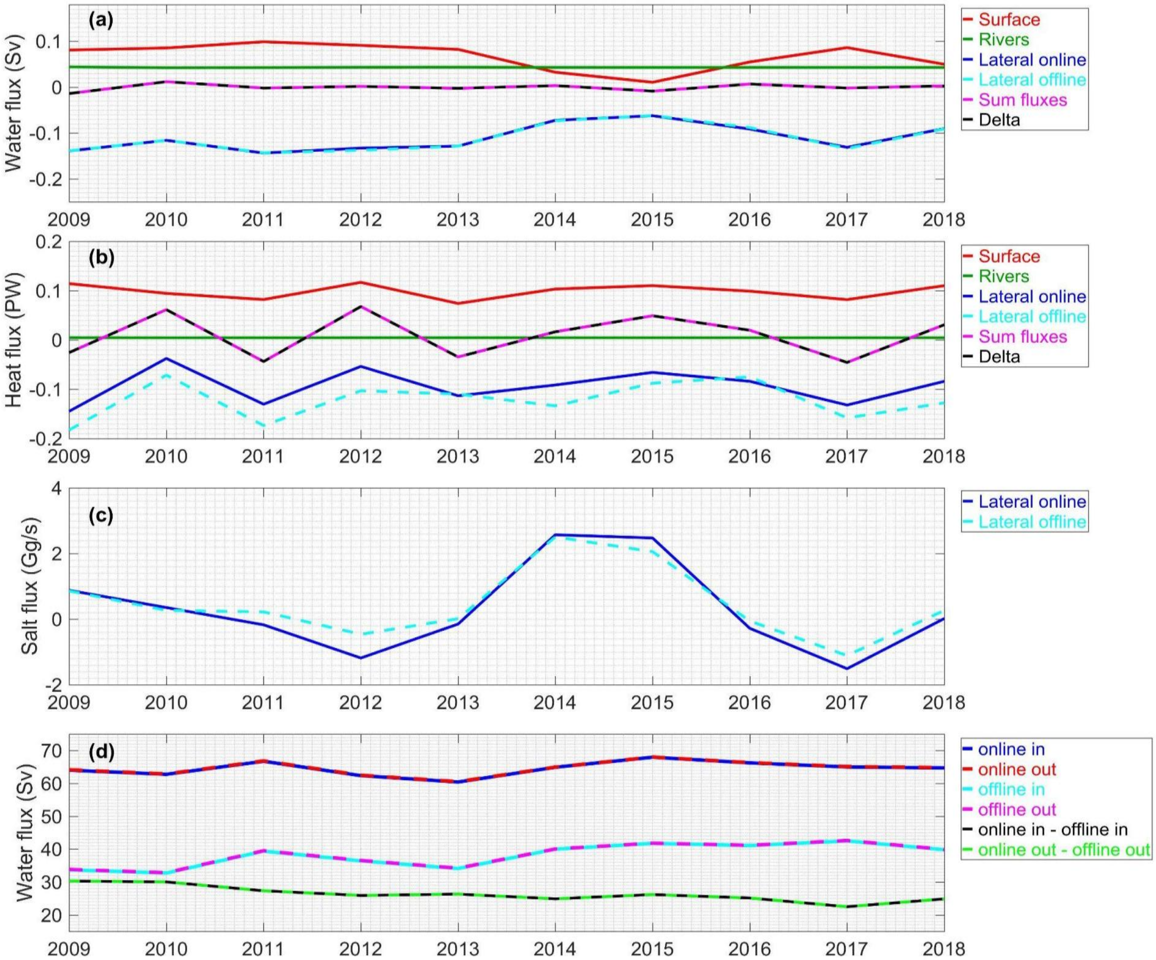


**Figure 8**: Atmospheric (surface, red), river (green) and net lateral (blue online, cyan offline) annual fluxes of (a) water, (b) heat and (c) salt and their sum (magenta), and annual variations of water, heat and salt contents (black) over the period 2009 - 2018; (d) Annual lateral inflow (blue online, cyan offline) and outflow (red online, magenta offline) of water volumes (in absolute values) computed online and offline, and the difference online - offline (black for inflow, green for outflow).

Third, the online computation allows us to compute separately the outflowing and inflowing terms of the lateral flux at each time step. Figure 8d shows the annual water lateral inflowing and outflowing fluxes (in absolute values) computed online and offline. Using the offline computational methods leads to important errors: the offline computation underestimates the water outflow and inflow by a factor of ~2 (Table 1). Correlations of online and

https://doi.org/10.5194/egusphere-2023-547
Preprint. Discussion started: 1 June 2023


offline water, heat and salt annual inflows or outflows are statistically significant (~ 0.80, p-value <0.01), showing a similar chronology in both methods. However, the bias between online and offline inflowing or outflowing lateral water, heat and salt fluxes is ~40% compared to the mean value, and high NRMSE values (~350%, 220% and 330% for water, heat and salt respectively) are obtained. These results quantitatively demonstrate the significant errors made when computing those fluxes offline and show the relevance of the online computation.

| Lateral flux | Mean value in online computation | Bias (offline - online) | Bias/mean (relative bias) in % | Correlation (offline/online) | NRMSE in % |
|---|---|---|---|---|---|
| Water net (Sv) | -0.1107 | -0.0004 | 0.4 | 1.00 (p=0.00) | 2 |
| Heat net (PW) | -0.094 | -0.029 | 30.5 | 0.86 (p=0.00) | 32 |
| Salt net (Gg/s) | 0.301 | 0.157 | 52.2 | 0.99 (p=0.00) | 8 |
| Water in (Sv) | 64.5 | -26.3 | 40.9 | 0.77 (p<0.01) | 351 |
| Water out (Sv) | -64.6 | 26.4 | 40.8 | 0.76 (p=0.01) | 354 |
| Heat in (PW) | 3.33 | -1.31 | 39.4 | 0.78 (p<0.01) | 220 |
| Heat out (PW) | -3.63 | 1.26 | 36.6 | 0.80 (p<0.01) | 229 |
| Salt in (Gg/s) | 2280 | -930 | 40.7 | 0.77 (p<0.01) | 336 |
| Salt out (Gg/s) | -2280 | 930 | 40.7 | 0.77 (p<0.01) | 339 |

**Table 1:** Mean values over 2009-2018 of water, heat and salt net, inflowing and outflowing annual fluxes through the SCS computed online (1st column), and absolute (2nd) and relative (3rd) bias, correlation (4th) and NRMSE (5th) between online and offline computations.

## 5. Conclusion

The three-dimensional hydrodynamic model SYMPHONIE was implemented over the South China Sea with high horizontal and vertical resolutions (4 km, 50 layers) to simulate and study the functioning, variability and influence of ocean circulation in the SCS and their role in regional climate.

A simulation was performed over the recent 10-year period 2009 – 2018, using three hourly atmospheric forcing, daily lateral oceanic boundary forcing, nine tidal forcing components and real-time or climatology data for 63 river discharge points. The ability of the model to reproduce the characteristics of circulation and water masses over the SCS was evaluated through a thorough comparison with available satellite and in-situ observation datasets. The model shows high similarity with surface satellite data and in-situ observations in terms of tidal representation and of seasonal

https://doi.org/10.5194/egusphere-2023-547
Preprint. Discussion started: 1 June 2023


cycle, interannual variability and spatial distribution of surface characteristics and circulation (SST, SSS, SLA and associated geostrophic currents), with low biases and highly significant spatial and temporal correlations. Comparisons with available Argo and glider in-situ temperature and salinity profiles showed that the model reproduces well the vertical distributions of temperature and salinity as well as MLD. These comparisons therefore quantitatively showed the realism of the representation of the spatial and temporal variability of the SCS circulation and water masses by this hydrodynamic model.

One of the first objectives of this numerical tool is to study the variability of the heat, water and salt budgets (and later carbon and nitrogen budgets) at different scales, precisely quantifying the contribution of each component involved in the budget equations: lateral, atmospheric and river fluxes, internal variations. For that, we developed an online computation of each term of those budgets that allowed to rigorously close them: over any given period, and for all the quantities studied (volume, heat and salt), the sum of all fluxes is rigorously equal to the variation of the quantity over the same period. We quantitatively demonstrated the added-value of the online method by assessing the error induced by an offline computation based on the use of daily temperature, salinity, volumes and currents outputs. NRMSE can be of the order of 10 to 30% for interannual variations of heat and salt net lateral fluxes. Moreover, this method allows to rigorously compute at each lateral section of interest (in particular straits) the inflowing and outflowing fluxes, contrary to the offline method that induces errors of the same order or even one order of magnitude larger than the online computed values themselves.

This 10-year simulation available over the SCS from a high-resolution model producing a consistent closed water, heat and salt budgets will be used to examine in detail the seasonal to interannual variability of the water, heat and salt budgets over the region. A decrease of SSS over the period 2011-2012 followed by an increase until 2016 were observed over the SCS (Zeng et al., 2014, 2018). Those interannual variations of SSS are well reproduced by our simulation. Zeng et al. (2014) suggested that an increase of precipitations and a reduced intrusion of the Kuroshio salty water mass were the main reasons for this minimum SSS over the SCS in 2012. Zeng et al. (2018) attributed the following SSS increase to limited precipitations and to a stronger Luzon inflow from the Pacific Ocean. Our simulation and online budget computation will be used in a coming paper to examine into detail the contribution of each term to those salinity variations over the area.

The simulation presented here is fully available to the interested scientific community. Using this hydrodynamical numerical tool to model and understand the SCS ocean dynamics will allow us to examine their influence on other compartments of the regional system. A coupling with a biogeochemical model (Herrmann et al., 2014, 2017) would allow to study the functioning and variability of SCS planktonic ecosystem, which are strongly influenced by ocean dynamics (Bombar et al., 2010; Loisel et al., 2017; Lu et al., 2018). This simulation, or simulation performed over given periods of interests, could also be used to assess the dispersion of potential contaminants over the area (plastics, radioactive contaminants, etc. e.g., Estournel et al., 2012). A coupling with a regional atmospheric model, that will allow to consider and examine the contributions of air-sea interactions in the ocean and atmosphere dynamics in the region, is also under development over the Southeast Asia region to be integrated in the framework of the CORDEX-SEA project (Tangang et al., 2020; Herrmann et al., 2022).

https://doi.org/10.5194/egusphere-2023-547
Preprint. Discussion started: 1 June 2023


**Code and data availability**

The SYMPHONIE hydrodynamical ocean model version 249, the SCS configuration, input files, data for model assessment and code used to generate figures are freely available on https://doi.org/10.5281/zenodo.7941495 (Trinh et al., 2023).

**Author contribution**

Trinh Bich Ngoc, Marine Herrmann and Caroline Ulses designed the experiments and Trinh Bich Ngoc carried them out, with the support of Thomas Duhaut, Patrick Marsaleix and Claude Estournel. Patrick Marsaleix, Thomas Duhaut and Claude Estournel developed the model code. Trinh Bich Ngoc, To Duy Thai, and Patrick Marsaleix worked on the model calibration and optimization. Trinh Bich Ngoc, Claude Estournel and Patrick Marsaleix implemented and analyzed the online and offline computational methods. R. Kipp Shearman organized the seaglider survey. Trinh Bich Ngoc, Marine Herrmann and Caroline Ulses prepared the manuscript with contributions from all coauthors.

**Competing interest**

The authors declare that they have no conflict of interest.

**Acknowledgments**

This work is a part of LOTUS international joint laboratory (lotus.usth.edu.vn). Numerical simulations were performed using CALMIP HPC facilities (project P13120) and the cluster OCCIGEN from the CINES group (project DARI A0080110098). Glider data were collected by the Vietnam Center for Oceanography (CFO, VASI) in the framework of the US-Vietnam collaboration project: "Gulf of Tonkin Circulation study" (NICOP N62909-15-1-2018), financed by the Office of Naval Research (ONR). This work is also supported by the Vietnam Academy of Science and Technology, grant code CSCL17.03/23-24.

**References**

Ablain, M., Cazenave, A., Larnicol, G., Balmaseda, M., Cipollini, P., Faugère, Y., Fernandes, M. J., Henry, O., Johannessen, J. A., Knudsen, P., Andersen, O., Legeais, J., Meyssignac, B., Picot, N., Roca, M., Rudenko, S., Scharffenberg, M. G., Stammer, D., Timms, G., and Benveniste, J.: Improved sea level record over the satellite altimetry era (1993–2010) from the Climate Change Initiative project, Ocean Science, 11, 67–82, https://doi.org/10.5194/os-11-67-2015, 2015.

Bombar, D., Dippner, J. W., Doan, H. N., Ngoc, L. N., Liskow, I., Loick-Wilde, N., and Voss, M.: Sources of new nitrogen in the Vietnamese upwelling region of the South China Sea, J Geophys Res Oceans, 115, https://doi.org/10.1029/2008JC005154, 2010.

Boutin, J., Martin, N., Kolodziejczyk, N., and Reverdin, G.: Interannual anomalies of SMOS sea surface salinity, Remote Sens Environ, 180, 128–136, https://doi.org/10.1016/j.rse.2016.02.053, 2016.

Carrere, L., Lyard, F., Cancet, M., Guillot, A., and Roblou, L.: FES 2012: a new global tidal model taking advantage of nearly 20 years of altimetry, 20 Years of Progress in Radar Altimetry, 2012.

https://doi.org/10.5194/egusphere-2023-547
Preprint. Discussion started: 1 June 2023


Chen, C. T. A., Hou, W. P., Gamo, T., and Wang, S. L.: Carbonate-related parameters of subsurface waters in the West Philippine, South China and Sulu Seas, Mar Chem, 99, 151–161, https://doi.org/10.1016/j.marchem.2005.05.008, 2006.

Chu, P. C. and Li, R.: South China Sea isopycnal-surface circulation, J Phys Oceanogr, 30, 2419–2438, https://doi.org/10.1175/1520-0485(2000)030<2419:SCSISC>2.0.CO;2, 2000.

Chung, S. W., Jan, S., and Liu, K. K.: Nutrient fluxes through the Taiwan Strait in spring and summer 1999, J Oceanogr, 57, https://doi.org/10.1023/A:1011122703552, 2001.

CIESIN: Gridded Population of the World, Version 4 (GPWv4): Basic Characteristics, Revision 11. Palisades, NY: NASA Socioeconomic Data and Applications Center (SEDAC)., Columbia University Center for International Earth Science Information Network (CIESIN) - Columbia University, 2018.

Costa, A., Doglioli, A. M., Marsaleix, P., and Petrenko, A. A.: Comparison of in situ microstructure measurements to different turbulence closure schemes in a 3-D numerical ocean circulation model, Ocean Model (Oxf), 120, https://doi.org/10.1016/j.ocemod.2017.10.002, 2017.

Da, N. D., Herrmann, M., Morrow, R., Niño, F., Huan, N. M., and Trinh, N. Q.: Contributions of Wind, Ocean Intrinsic Variability, and ENSO to the Interannual Variability of the South Vietnam Upwelling: A Modeling Study, J Geophys Res Oceans, 124, 6545–6574, https://doi.org/10.1029/2018JC014647, 2019.

Estournel, C., Bosc, E., Bocquet, M., Ulses, C., Marsaleix, P., Winiarek, V., Osvath, I., Nguyen, C., Duhaut, T., Lyard, F., Michaud, H., and Auclair, F.: Assessment of the amount of cesium-137 released into the Pacific Ocean after the Fukushima accident and analysis of its dispersion in Japanese coastal waters, J Geophys Res Oceans, 117, https://doi.org/10.1029/2012JC007933, 2012.

Estournel, C., Marsaleix, P., and Ulses, C.: A new assessment of the circulation of Atlantic and Intermediate Waters in the Eastern Mediterranean, Prog Oceanogr, 198, https://doi.org/10.1016/j.pocean.2021.102673, 2021.

Fang, G., Zhao, B., and Zhu, Y.: Water volume transport through the taiwan strait and the continental skelf of the east china sea measured with current meters, Elsevier Oceanography Series, 54, 345–358, https://doi.org/10.1016/S0422-9894(08)70107-7, 1991.

Fang, G., Susanto, D., Soesilo, I., Zheng, Q., Qiao, F., and Wei, Z.: A note on the South China Sea shallow interocean circulation, Adv Atmos Sci, 22, 946–954, https://doi.org/10.1007/bf02918693, 2005.

Fang, G., Wang, Y., Wei, Z., Fang, Y., Qiao, F., and Hu, X.: Interocean circulation and heat and freshwater budgets of the South China Sea based on a numerical model, Dynamics of Atmospheres and Oceans, 47, 55–72, https://doi.org/10.1016/j.dynatmoce.2008.09.003, 2009.

https://doi.org/10.5194/egusphere-2023-547
Preprint. Discussion started: 1 June 2023


Fang, G., Susanto, R. D., Wirasantosa, S., Qiao, F., Supangat, A., Fan, B., Wei, Z., Sulistiyo, B., and Li, S.: Volume, heat, and freshwater transports from the South China Sea to Indonesian seas in the boreal winter of 2007-2008, J Geophys Res Oceans, 115, 1–11, https://doi.org/10.1029/2010JC006225, 2010.

Gan, J., Li, H., Curchitser, E. N., and Haidvogel, D. B.: Modeling South China Sea circulation: Response to seasonal forcing regimes, J Geophys Res Oceans, 111, 1–20, https://doi.org/10.1029/2005JC003298, 2006.

Gan, J., Liu, Z., and Hui, C. R.: A three-layer alternating spinning circulation in the South China Sea, J Phys Oceanogr, 46, 2309–2315, https://doi.org/10.1175/JPO-D-16-0044.1, 2016.

Garau, B., Ruiz, S., Zhang, W. G., Pascual, A., Heslop, E., Kerfoot, J., and Tintoré, J.: Thermal lag correction on slocum CTD glider data, J Atmos Ocean Technol, 28, https://doi.org/10.1175/JTECH-D-10-05030.1, 2011.

Gordon, A. L., Tessler, Z. D., and Villanoy, C.: Dual overflows into the deep Sulu Sea, Geophys Res Lett, 38, 1–6, https://doi.org/10.1029/2011GL048878, 2011.

Griffies, S. M. and Hallberg, R. W.: Biharmonic friction with a Smagorinsky-like viscosity for use in large-scale eddy-permitting ocean models, Mon Weather Rev, 128, https://doi.org/10.1175/1520-0493(2000)128<2935:bfwasl>2.0.co;2, 2000.

Guohong, F.: Tide and tidal current charts for the marginal seas adjacent to China, Chinese Journal of Oceanology and Limnology, 4, https://doi.org/10.1007/BF02850393, 1986.

Herrmann, M., Estournel, C., Adloff, F., and Diaz, F.: Impact of climate change on the northwestern Mediterranean Sea pelagic planktonic ecosystem and associated carbon cycle, J Geophys Res Oceans, 119, https://doi.org/10.1002/2014JC010016, 2014.

Herrmann, M., Auger, P. A., Ulses, C., and Estournel, C.: Long-term monitoring of ocean deep convection using multisensors altimetry and ocean color satellite data, J Geophys Res Oceans, 122, https://doi.org/10.1002/2016JC011833, 2017.

Herrmann, M., Nguyen-Duy, T., Ngo-Duc, T., and Tangang, F.: Climate change impact on sea surface winds in Southeast Asia, International Journal of Climatology, 42, https://doi.org/10.1002/joc.7433, 2022.

Herrmann, M., To Duy, T., and Estournel, C.: Intraseasonal variability of the South Vietnam Upwelling, South China Sea: influence of atmospheric forcing and ocean intrinsic variability, EGUsphere [preprint], https://doi.org/10.5194/egusphere-2022-1443, 2023

Ho, C. R., Zheng, Q., Soong, Y. S., Kuo, N. J., and Hu, J. H.: Seasonal variability of sea surface height in the South China Sea observed with TOPEX/Poseidon altimeter data, J Geophys Res Oceans, 105, 13981–13990, https://doi.org/10.1029/2000jc900001, 2000.

https://doi.org/10.5194/egusphere-2023-547
Preprint. Discussion started: 1 June 2023


Hsin, Y. C., Wu, C. R., and Chao, S. Y.: An updated examination of the Luzon Strait transport, J Geophys Res Oceans, 117, https://doi.org/10.1029/2011JC007714, 2012.

Jackett, D. R., McDougall, T. J., Feistel, R., Wright, D. G., and Griffies, S. M.: Algorithms for density, potential temperature, conservative temperature, and the freezing temperature of seawater, J Atmos Ocean Technol, 23, 1709–1728, https://doi.org/10.1175/JTECH1946.1, 2006.

Kumar, A., Jha, B., and L'Heureux, M.: Are tropical SST trends changing the global teleconnection during La Niña?, Geophys Res Lett, 37, https://doi.org/10.1029/2010GL043394, 2010.

Leonard, B. P.: A stable and accurate convective modelling procedure based on quadratic upstream interpolation, Comput Methods Appl Mech Eng, 19, https://doi.org/10.1016/0045-7825(79)90034-3, 1979.

Lin, H., Liu, Z., Hu, J., Menemenlis, D., and Huang, Y.: Characterizing meso- to submesoscale features in the South China Sea, Prog Oceanogr, 188, https://doi.org/10.1016/j.pocean.2020.102420, 2020.

Liu, K. K., Chao, S. Y., Shaw, P. T., Gong, G. C., Chen, C. C., and Tang, T. Y.: Monsoon-forced chlorophyll distribution and primary production in the South China Sea: Observations and a numerical study, Deep Sea Res 1 Oceanogr Res Pap, 49, 1387–1412, https://doi.org/10.1016/S0967-0637(02)00035-3, 2002.

Liu, K. K., Kang, C. K., Kobari, T., Liu, H., Rabouille, C., and Fennel, K.: Biogeochemistry and ecosystems of continental margins in the western North Pacific Ocean and their interactions and responses to external forcing - An overview and synthesis, Biogeosciences, 11, 7061–7075, https://doi.org/10.5194/bg-11-7061-2014, 2014.

Liu, Q., Kaneko, A., and Jilan, S.: Recent progress in studies of the South China Sea circulation, https://doi.org/10.1007/s10872-008-0063-8, 2008.

Liu, Q., Feng, M., and Wang, D.: ENSO-induced interannual variability in the southeastern South China Sea, J Oceanogr, 67, 127–133, https://doi.org/10.1007/s10872-011-0002-y, 2011.

Liu, Y., Tang, D., and Evgeny, M.: Chlorophyll concentration response to the typhoon wind-pump induced upper ocean processes considering air-sea heat exchange, Remote Sens (Basel), 11, https://doi.org/10.3390/rs11151825, 2019.

Liu, Z. and Gan, J.: Three-dimensional pathways of water masses in the South China Sea: A modeling study, J Geophys Res Oceans, 122, https://doi.org/10.1002/2016JC012511, 2017.

Loisel, H., Vantrepotte, V., Ouillon, S., Ngoc, D. D., Herrmann, M., Tran, V., Mériaux, X., Dessailly, D., Jamet, C., Duhaut, T., Nguyen, H. H., and van Nguyen, T.: Assessment and analysis of the chlorophyll-a concentration variability over the Vietnamese coastal waters from the MERIS ocean color sensor (2002–2012), Remote Sens Environ, 190, 217–232, https://doi.org/10.1016/j.rse.2016.12.016, 2017.

https://doi.org/10.5194/egusphere-2023-547
Preprint. Discussion started: 1 June 2023


Lu, W., Oey, L. Y., Liao, E., Zhuang, W., Yan, X. H., and Jiang, Y.: Physical modulation to the biological productivity in the summer Vietnam upwelling system, Ocean Science, 14, https://doi.org/10.5194/os-14-1303-2018, 2018.

Lyard, F., Lefevre, F., Letellier, T., and Francis, O.: Modelling the global ocean tides: Modern insights from FES2004, Ocean Dyn, 56, https://doi.org/10.1007/s10236-006-0086-x, 2006.

Marsaleix, P., Auclair, F., and Estournel, C.: Considerations on open boundary conditions for regional and coastal ocean models, J Atmos Ocean Technol, 23, 1604–1613, https://doi.org/10.1175/JTECH1930.1, 2006.

Marsaleix, P., Auclair, F., Floor, J. W., Herrmann, M. J., Estournel, C., Pairaud, I., and Ulses, C.: Energy conservation issues in sigma-coordinate free-surface ocean models, Ocean Model (Oxf), 20, 61–89, https://doi.org/10.1016/j.ocemod.2007.07.005, 2008.

Marsaleix, P., Auclair, F., and Estournel, C.: Low-order pressure gradient schemes in sigma coordinate models: The seamount test revisited, Ocean Model (Oxf), 30, 169–177, https://doi.org/10.1016/j.ocemod.2009.06.011, 2009.

Marsaleix, P., Michaud, H., and Estournel, C.: 3D phase-resolved wave modelling with a non-hydrostatic ocean circulation model, Ocean Model (Oxf), 136, 28–50, https://doi.org/10.1016/j.ocemod.2019.02.002, 2019.

Metzger, E. J. and Hurlburt, H. E.: Coupled dynamics of the South China Sea, the Sulu Sea, and the Pacific Ocean, J Geophys Res Oceans, 101, 12331–12352, https://doi.org/10.1029/95JC03861, 1996.

Nan, F., Xue, H., and Yu, F.: Kuroshio intrusion into the South China Sea: A review, Prog Oceanogr, 137, 314–333, https://doi.org/10.1016/j.pocean.2014.05.012, 2015.

Nguyen-Duy, T., Ayoub, N. K., Marsaleix, P., Toublanc, F., de Mey-Frémaux, P., Piton, V., Herrmann, M., Duhaut, T., Tran, M. C., and Ngo-Duc, T.: Variability of the Red River Plume in the Gulf of Tonkin as Revealed by Numerical Modeling and Clustering Analysis, Front Mar Sci, 8, https://doi.org/10.3389/fmars.2021.772139, 2021.

Ni, Q., Zhai, X., Wilson, C., Chen, C., and Chen, D.: Submesoscale Eddies in the South China Sea, Geophys Res Lett, 48, https://doi.org/10.1029/2020GL091555, 2021.

Pairaud, I. L., Lyard, F., Auclair, F., Letellier, T., and Marsaleix, P.: Dynamics of the semi-diurnal and quarter-diurnal internal tides in the Bay of Biscay. Part 1: Barotropic tides, Cont Shelf Res, 28, https://doi.org/10.1016/j.csr.2008.03.004, 2008.

Pairaud, I. L., Auclair, F., Marsaleix, P., Lyard, F., and Pichon, A.: Dynamics of the semi-diurnal and quarter-diurnal internal tides in the Bay of Biscay. Part 2: Baroclinic tides, Cont Shelf Res, 30, https://doi.org/10.1016/j.csr.2009.10.008, 2010.

https://doi.org/10.5194/egusphere-2023-547
Preprint. Discussion started: 1 June 2023


Pan, J. and Sun, Y.: Estimate of ocean mixed layer deepening after a typhoon passage over the south china sea by using satellite data, J Phys Oceanogr, 43, 498–506, https://doi.org/10.1175/JPO-D-12-01.1, 2013.

Penjan, R., Siriporn, P., and Natinee, N.: Temperature , Salinity , Dissolved Oxygen and Water Masses of Vietnamese Waters, Proceeding of the SEAFDEC Seminar on Fisheries resources in the South China Sea area IV, Vietnamese Waters. Thailand: South- east Asian Fisheries Development Center, 346–355, 1997.

Piton, V., Herrmann, M., Lyard, F., Marsaleix, P., Duhaut, T., Allain, D., and Ouillon, S.: Sensitivity study on the main tidal constituents of the Gulf of Tonkin by using the frequency-domain tidal solver in T-UGOm, Geosci Model Dev, 13, 1583–1607, https://doi.org/10.5194/gmd-13-1583-2020, 2020.

Qu, T.: Upper-layer circulation in the South China Sea, J Phys Oceanogr, 30, 1450–1460, https://doi.org/10.1175/1520-0485(2000)030<1450:ULCITS>2.0.CO;2, 2000.

Qu, T. and Song, Y. T.: Mindoro Strait and Sibutu Passage transports estimated from satellite data, Geophys Res Lett, 36, 1–5, https://doi.org/10.1029/2009GL037314, 2009.

Qu, T., Kim, Y. Y., Yaremchuk, M., Tuzuka, T., Ishida, A., and Yamagata, T.: Can Luzon Strait transport play a role in conveying the impact of ENSO to the South China Sea?, J Clim, 17, 3644–3657, https://doi.org/10.1175/1520-0442(2004)017<3644:CLSTPA>2.0.CO;2, 2004.

Qu, T., Du, Y., Meyers, G., Ishida, A., and Wang, D.: Connecting the tropical Pacific with Indian Ocean through South China Sea, Geophys Res Lett, 32, 1–4, https://doi.org/10.1029/2005GL024698, 2005.

Qu, T., Du, Y., and Sasaki, H.: South China Sea throughflow: A heat and freshwater conveyor, Geophys Res Lett, 33, https://doi.org/10.1029/2006GL028350, 2006.

Ray, R. D. and Zaron, E. D.: M2 internal tides and their observed wavenumber spectra from satellite altimetry, J Phys Oceanogr, 46, https://doi.org/10.1175/JPO-D-15-0065.1, 2016.

Rogowski, P., Zavala-Garay, J., Shearman, K., Terrill, E., Wilkin, J., and Lam, T. H.: Air-Sea-Land Forcing in the Gulf of Tonkin: Assessing seasonal variability using modern tools, Oceanography, 32, https://doi.org/10.5670/oceanog.2019.223, 2019.

Rojana-anawat, P., Sukramongkol, N., and Pradit, S.: Characteristics of Water in the South China Sea , Area III : Western Philippines, Characteristics of Water in the South China Sea, Area III: Western Philippines, 291–307, 1998.

Saadon, M. N., Rojana-Anawat, P., and Snidvongs, A.: Physical Characteristics of Watermass in the South China Sea , Area I : Gulf of Thailand and East Coast of Peninsular Malaysia, Proceedings of the Second Technical Seminar on Marine Fishery Resources Survey in the South China Sea, Area II: Sarawak, Sabah and Brunei Darussalam Waters, 1–5, 1998a.

https://doi.org/10.5194/egusphere-2023-547
Preprint. Discussion started: 1 June 2023


Saadon, M. N., Kin, L. P., Snidvongs, A., and Rojana-Anawat, P.: Physical Characteristics of Watermass in the South China Sea , Area II : Sarawak, Sabah and Brunei Darussalam Waters, Proceedings of the Second Technical Seminar on Marine Fishery Resources Survey in the South China Sea, Area II: Sarawak, Sabah and Brunei Darussalam Waters, 1–22, 1998b.

Shaw, P. T. and Chao, S. Y.: Surface circulation in the South China Sea, Deep-Sea Research Part I, 41, 1663–1683, https://doi.org/10.1016/0967-0637(94)90067-1, 1994.

Shaw, P. T., Chao, S. Y., and Fu, L. L.: Sea surface height variations in the South China Sea from satellite altimetry, Oceanologica Acta, 22, 1–17, https://doi.org/10.1016/S0399-1784(99)80028-0, 1999.

Soden, B. J., Lau, N.-C., and Klein, S. A.: Remote Sea Surface Temperature Variations during ENSO: Evidence for a Tropical Atmospheric Bridge, J Clim, 12, 917–932, 1999.

Sprintall, J., Gordon, A. L., Flament, P., and Villanoy, C. L.: Observations of exchange between the South China Sea and the Sulu Sea, J Geophys Res Oceans, 117, 1–18, https://doi.org/10.1029/2011JC007610, 2012.

Susanto, R. D., Wei, Z., Adi, R. T., Fan, B., Li, S., and Fang, G.: Observations of the Karimata Strait througflow from December 2007 to November 2008, Acta Oceanologica Sinica, 32, 1–6, https://doi.org/10.1007/s13131-013-0307-3, 2013.

Talley, L. D., Pickard, G. L., Emery, W. J., and Swift, J. H.: Descriptive physical oceanography: An introduction: Sixth edition, https://doi.org/10.1016/C2009-0-24322-4, 2011.

Tan, W., Wang, X., Wang, W., Wang, C., and Zuo, J.: Different responses of sea surface temperature in the South China Sea to various El Niño events during boreal autumn, J Clim, 29, 1127–1142, https://doi.org/10.1175/JCLI-D-15-0338.1, 2016.

Tangang, F., Chung, J. X., Juneng, L., Supari, Salimun, E., Ngai, S. T., Jamaluddin, A. F., Mohd, M. S. F., Cruz, F., Narisma, G., Santisirisomboon, J., Ngo-Duc, T., van Tan, P., Singhruck, P., Gunawan, D., Aldrian, E., Sopaheluwakan, A., Grigory, N., Remedio, A. R. C., Sein, D. v., Hein-Griggs, D., McGregor, J. L., Yang, H., Sasaki, H., and Kumar, P.: Projected future changes in rainfall in Southeast Asia based on CORDEX–SEA multi-model simulations, Clim Dyn, 55, https://doi.org/10.1007/s00382-020-05322-2, 2020.

Tian, J., Yang, Q., Liang, X., Xie, L., Hu, D., Wang, F., and Qu, T.: Observation of Luzon Strait transport, Geophys Res Lett, 33, 1–6, https://doi.org/10.1029/2006GL026272, 2006.

To Duy, T., Herrmann, M., Estournel, C., Marsaleix, P., Duhaut, T., Bui Hong, L., and Trinh Bich, N.: Role of wind, mesoscale dynamics and coastal circulation in the interannual variability of South Vietnam Upwelling, South China Sea. Answers from a high resolution ocean model, https://doi.org/10.5194/os-2021-121, n.d.

https://doi.org/10.5194/egusphere-2023-547
Preprint. Discussion started: 1 June 2023


Tozuka, T., Qu, T., and Yamagata, T.: Dramatic impact of the South China Sea on the Indonesian throughflow, Geophys Res Lett, 34, 3–7, https://doi.org/10.1029/2007GL030420, 2007.

Tozuka, T., Qu, T., and Yamagata, T.: Impacts of South China Sea throughflow on the mean state and El Niño/Southern Oscillation as revealed by a coupled GCM, J Oceanogr, 71, 105–114, https://doi.org/10.1007/s10872-014-0265-1, 2015.

Tranchant, B., Reffray, G., Greiner, E., Nugroho, D., Koch-Larrouy, A., and Gaspar, P.: Evaluation of an operational ocean model configuration at 1/12° spatial resolution for the Indonesian seas (NEMO2.3/INDO12); Part 1: Ocean physics, Geosci Model Dev, 9, 1037–1064, https://doi.org/10.5194/gmd-9-1037-2016, 2016.

Trinh, N. B., Marsaleix, P., Estournel, C., Herrmann, M., Ulses, C., Duhaut, T., Shearman, R. K., and To-Duy, T.: High-resolution configuration of the hydrodynamical ocean model SYMPHONIE (version 249) over the South China Sea, https://doi.org/10.5281/ZENODO.7941495, 2023.

Uu, D. v. and Brankart, J. M.: Seasonal variation of temperature and salinity fields and water masses in the Bien Dong (South China) Sea, Math Comput Model, 26, 97–113, https://doi.org/10.1016/S0895-7177(97)00243-4, 1997.

Wang, C., Wang, W., Wang, D., and Wang, Q.: Interannual variability of the South China Sea associated with El Niño, J Geophys Res Oceans, 111, https://doi.org/10.1029/2005JC003333, 2006a.

Wang, G., Su, J., Ding, Y., and Chen, D.: Tropical cyclone genesis over the south China sea, Journal of Marine Systems, 68, 318–326, https://doi.org/10.1016/j.jmarsys.2006.12.002, 2007.

Wang, Q., Cui, H., Zhang, S., and Hu, D.: Water transports through the four main straits around the South China Sea, Chinese Journal of Oceanology and Limnology, 27, 229–236, https://doi.org/10.1007/s00343-009-9142-y, 2009.

Wang, Y., Fang, G., Wei, Z., Qiao, F., and Chen, H.: Interannual variation of the South China Sea circulation and its relation to El Niño, as seen from a variable grid global ocean model, J Geophys Res Oceans, 111, 1–15, https://doi.org/10.1029/2005JC003269, 2006b.

Wang, Y., Xu, T., Li, S., Susanto, R. D., Agustiadi, T., Trenggono, M., Tan, W., and Wei, Z.: Seasonal variation of water transport through the Karimata Strait, Acta Oceanologica Sinica, 38, 47–57, https://doi.org/10.1007/s13131-018-1224-2, 2019.

Wang, Y. H., Jan, S., and Wang, D. P.: Transports and tidal current estimates in the Taiwan Strait from shipboard ADCP observations (1999-2001), Estuar Coast Shelf Sci, 57, 193–199, https://doi.org/10.1016/S0272-7714(02)00344-X, 2003.

https://doi.org/10.5194/egusphere-2023-547
Preprint. Discussion started: 1 June 2023


Wei, J., Li, M. T., Malanotte-Rizzoli, P., Gordon, A. L., and Wang, D. X.: Opposite variability of indonesian throughflow and south china sea throughflow in the Sulawesi Sea, J Phys Oceanogr, 46, 3165–3180, https://doi.org/10.1175/JPO-D-16-0132.1, 2016.

Wyrtki, K.: Physical Oceanography of the Southeast Asian Waters. Naga Report Volume 2. Scientific Results of Marine Investigation of the South China Sea and the Gulf of Thailand 1959-1961, Scientific Results of Marine Investigation of the South China Sea and the Gulf of Thailand 1959-1961, 2, 195, 1961.

Yang, H., Liu, Q., and Jia, X.: On the Upper Oceanic Heat Budget in the South China Sea: Annual Cycle, Adv Atmos Sci, 16, 619–629, https://doi.org/10.1007/s00376-999-0036-x, 1999.

Yaremchuk, M., McCreary, J., Yu, Z., and Furue, R.: The South China Sea through flow retrieved from climatological data, J Phys Oceanogr, 39, 753–767, https://doi.org/10.1175/2008JPO3955.1, 2009.

Yu, K. and Qu, T.: Imprint of the pacific decadal oscillation on the South China Sea throughflow variability, J Clim, 26, https://doi.org/10.1175/JCLI-D-12-00785.1, 2013.

Yu, L. and Weller, R. A.: Objectively analyzed air-sea heat fluxes for the global ice- free oceans (1981-2005), Bull Am Meteorol Soc, 88, 527–539, https://doi.org/10.1175/BAMS-88-4-527, 2007.

Yu, Y., Zhang, H. R., Jin, J., and Wang, Y.: Trends of sea surface temperature and sea surface temperature fronts in the South China Sea during 2003–2017, Acta Oceanologica Sinica, 38, 106–115, https://doi.org/10.1007/s13131-019-1416-4, 2019.

Yu, Z., Shen, S., McCreary, J. P., Yaremchuk, M., and Furue, R.: South China Sea throughflow as evidence by satellite images and numerical experiments, Geophys Res Lett, 34, 2–7, https://doi.org/10.1029/2006GL028103, 2007.

Yuan, Y., Liao, G., and Yang, C.: The Kuroshio near the Luzon Strait and circulation in the northern South China Sea during August and September 1994, J Oceanogr, 64, 777–788, https://doi.org/10.1007/s10872-008-0065-6, 2008.

Zeng, L., Timothy Liu, W., Xue, H., Xiu, P., and Wang, D.: Freshening in the South China Sea during 2012 revealed by Aquarius and in situ data, J Geophys Res Oceans, 119, https://doi.org/10.1002/2014JC010108, 2014.

Zeng, L., Chassignet, E. P., Schmitt, R. W., Xu, X., and Wang, D.: Salinification in the South China Sea Since Late 2012: A Reversal of the Freshening Since the 1990s, Geophys Res Lett, 45, https://doi.org/10.1002/2017GL076574, 2018.